

Phononic enhancement and detection of hidden spin-nematicity and dynamics in quantum magnets

Junyu Tang,¹ Hong-Hao Song,¹ and Gang v. Chen^{1,2,*}

¹*International Center for Quantum Materials, School of Physics, Peking University, Beijing 100871, China*

²*Collaborative Innovation Center of Quantum Matter, 100871, Beijing, China*

The spin nematic phase, characterized by long-range order of spin quadrupole moments in the absence of dipolar magnetism, presents a significant challenge for conventional experimental detection. We propose a novel method to detect this elusive order in quantum magnets with an illustration in the spin-1 triangular lattice Mott insulator. By integrating out the phonon degrees of freedom, we obtain a phase diagram with substantially enlarged regions for the spin-nematic and spin-nematic-supersolid phases. We then demonstrate that through the spin-lattice coupling, the emergence of spin nematic order imprints a distinctive signature onto the phonon spectra, providing a clear spectroscopic signature for the quadrupolar order accessible via Raman or inelastic X-ray scattering. Our formalism offers a direct and powerful method to uncover the hidden spin nematicity, opening a new pathway for diagnosing multipolar orders in quantum magnets.

Quantum magnets with the spin moments greater than 1/2 can host exotic phases of matter that extend beyond traditional magnetic order [1, 2]. For higher spin systems, the local moments are characterized not only by a dipole moment but also by the multipole moment such as the quadrupole moment [3–5]. The ordering of these quadrupole moments leads to a spin nematic phase [6–10], a quantum paramagnetic state analogous to the liquid crystals, where the conventional magnetic dipolar order is absent but the spin system spontaneously breaks the rotational symmetry in the spin space.

A major obstacle in the study of the spin nematics is the difficulty in detecting them experimentally [11–13]. Since the neutron scattering primarily couples to the magnetic dipole moments [14, 15], it is largely blind to the purely quadrupolar orders that are even under time reversal. While recent progress proposed that quadrupolar excitations could become visible in inelastic neutron scattering [5], it requires the hybridization between one- and two-magnon channels. Moreover, this route still fundamentally relies on the spin-excitation spectrum. Here, we instead pursue an innovative phonon-based route, where bond phonons are not only a probe but also an active mechanism that enhance the stability of the spin-nematicity. Specifically, the emergence of spin nematic order imprints a distinctive signature onto the phonon spectrum through the spin-lattice coupling, providing a clear pathway for the detection of the hidden quadrupolar order.

We first demonstrate that the magnetoelastic couplings can substantially enhance and stabilize the spin nematic phase due to an induced biquadratic spin interaction. Then, we show that the emergence of quadrupolar order in the spin-nematic phase manifests itself in the phonon spectrum through two primary signatures, a pronounced phonon frequency splitting (an avoided crossing between phonon and magnon bands) and a strong dependence of the splitting position on the background spin-nematic order and the external magnetic field. Spectroscopic techniques such as Raman spectroscopy [16, 17], inelastic X-ray scattering [18, 19] are ideally suited to detect these changes, thereby translating the hidden spin order into an observable lattice response and offering a direct solution to the long-standing challenge of probing spin nematics. Our proposal is supported by both contemporary theoretical

and experimental landscapes. Theoretically, the formation of the spin nematic phase via the condensation of two-magnon bound states is well established [5, 9, 20, 21], with models highlighting the important role of anisotropy and frustration on the triangular lattice. Experimentally, the spin nematic order and two-magnon Bose-Einstein condensate have been reported in a growing set of candidate materials [12, 13, 22, 23], providing various platforms to test our proposal.

We start with a spin-1 XXZ model in a triangular lattice with the magnetoelastic interaction, where the lattice modulates the exchange couplings through vibrations. This framework will be used in two complementary ways, (i) integrating out the phonons to obtain an effective spin model and investigate how the spin-lattice coupling reshapes the spin states, and (ii) retaining phonons to compute the spectra with dynamical magnon-phonon couplings that provide the spectroscopic signatures of hidden spin nematicity [24]. Our model is written as

$$H = H_s + H_p + H_{me}, \quad (1)$$

where H_s and H_p are the spin and phonon Hamiltonian, respectively. H_{me} describes the magnetoelastic effect that characterizes the magnon-phonon interaction. The spin Hamiltonian includes a magnetic field B and a large single-ion easy-axis anisotropy with $D > 0$ in addition to the XXZ anisotropy,

$$H_s = J \sum_{\langle i,j \rangle} (S_i^x S_j^x + S_i^y S_j^y + \Delta S_i^z S_j^z) - D \sum_i (S_i^z)^2 - B \sum_i S_i^z. \quad (2)$$

The exchange interaction is restricted between the nearest-neighbor sites with antiferromagnetic coupling $J > 0$. Δ characterizes the XXZ anisotropy. In the model, we assume a large easy-axis anisotropy, which is often required for the emergence of on-site two-magnon bound state [22]. A moderate XXZ Ising anisotropy $\Delta > 1$ is chosen. As for the phonon Hamiltonian H_p , in the bond-phonon model it takes the form

$$H_p = \sum_i \frac{|\mathbf{p}_i|^2}{2M} + \frac{k_E}{2} \sum_{\langle i,j \rangle} (\mathbf{e}_{ij} \cdot \mathbf{u}_{ij})^2, \quad (3)$$

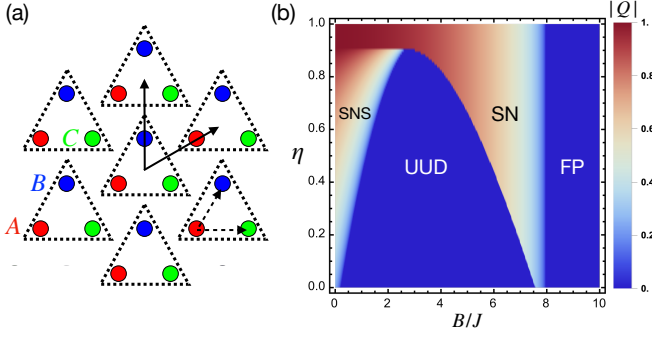


FIG. 1. (a) Triangular lattice structure with ordering wavevector at K where a unit cell (dashed lines) contains three sublattices as colored in red (A), blue (B) and green (C). The black solid (dashed) arrows are the lattice vectors for the supercell (original triangular lattice). (b) Phase diagram of H_s^{eff} in (6) with the averaged quadrupolar order $|Q| \equiv \sum_{\alpha \in \{A,B,C\}} [\langle Q_{\alpha}^{x^2-y^2} \rangle^2 + \langle Q_{\alpha}^{xy} \rangle^2]^{1/2}/3$. Here and in the following, $D = 4J$ and $\Delta = 1.2$ are used in the calculation.

where M and \mathbf{p}_i are the mass and momentum of the magnetic atom, respectively. $\mathbf{u}_{ij} \equiv \mathbf{u}_i - \mathbf{u}_j$ is the in-plane lattice displacement and \mathbf{e}_{ij} is the unit vector connecting sites i and j . k_E is the spring constant $k_E = M\omega_0^2$ with ω_0 the intrinsic vibration frequency.

The magnetoelastic interaction can be obtained by expanding the exchange coupling with respect to the lattice distance \mathbf{R}_{ij} around the equilibrium position \mathbf{R}_{ij}^0 [25, 26], where $J(\mathbf{R}_{ij} + \mathbf{u}_{ij}) \approx J(\mathbf{R}_{ij}^0) - \frac{\partial J}{\partial \mathbf{R}} \mathbf{e}_{ij} \cdot \mathbf{u}_{ij} \equiv J(1 - \gamma \mathbf{e}_{ij} \cdot \mathbf{u}_{ij})$. Therefore, the magnetoelastic interaction can be written as

$$H_{me} = -J\gamma \sum_{\langle i,j \rangle} \mathbf{e}_{ij} \cdot \mathbf{u}_{ij} (S_i^x S_j^x + S_i^y S_j^y + \Delta S_i^z S_j^z). \quad (4)$$

Here, the expansion coefficient $\gamma = (\partial_R J)/J$ is positive since the exchange usually decreases with increasing bond length.

Enhanced spin nematicity.—To explore the phonon effect on the spin states, we integrate out the phonons \mathbf{u}_{ij} , that enters the Hamiltonian quadratically in H_p and linearly in H_{me} . Consequently, the phonon field can be eliminated analytically via Gaussian integration [25, 27], resulting in a bilinear–biquadratic Hamiltonian

$$H_s^{\text{eff}} = J \sum_{\langle i,j \rangle} (S_i^x S_j^x + S_i^y S_j^y + \Delta S_i^z S_j^z) - D \sum_i (S_i^z)^2 - B \sum_i S_i^z - J\eta \sum_{\langle i,j \rangle} (S_i^x S_j^x + S_i^y S_j^y + \Delta S_i^z S_j^z)^2, \quad (5)$$

where a biquadratic term emerges with the strength $J\eta \equiv J\eta$. Here, the dimensionless magnetoelastic coupling coefficient is defined as $\eta = J\gamma^2/k_E$. While such biquadratic term is known to be essential for the quadrupolar spin order [28–30], pinning down its precise microscopic origin in real materials remains a challenge. Various mechanisms have been suggested, ranging from the twisted ring exchange [31], higher-order perturbation from spin-charge coupling [32, 33], virtual crystal field

fluctuations [34] and multipolar interactions [35]. Here, the biquadratic term in Eq. (5) arises naturally from magnetoelastic interactions [25, 36].

To clarify how the quadrupolar order emerges from the effective model in Eq. (5), we further project out the high-energy $|S^z = 0\rangle$ state to establish a low-energy effective model in the manifold of $\{|\uparrow\rangle \equiv |S^z = +1\rangle, |\downarrow\rangle \equiv |S^z = -1\rangle\}$, that is demanded by the easy-axis single-ion anisotropy. Within this two-fold local Hilbert space [5], the pseudospin operators τ are introduced with $\tau^z = PS^zP/2$, $\tau^{\pm} = P(S^{\pm})^2P/2$, where $S^{\pm} = S^x \pm iS^y$, $\tau^{\pm} = \tau^x \pm i\tau^y$, and $P = |\uparrow\rangle\langle\uparrow| + |\downarrow\rangle\langle\downarrow|$ is the projection operator for the pseudospin-1/2 space. It is obvious that $PS^{x,y}P = 0$. Therefore, if we directly project the Hamiltonian (5) for each site, the pairwise exchange term $S_i^x S_j^x + S_i^y S_j^y$ will not survive. However, such one-magnon process can be treated as perturbation and after a Schrieffer–Wolff transformation for projecting into the low-energy space, it becomes biquadratic [27], which has the same form as the last term in Hamiltonian (5). The final effective Hamiltonian then takes the form [27]

$$H_s^{\text{eff}} = \sum_{\langle i,j \rangle} \left[J_{xy} (\tau_i^x \tau_j^x + \tau_i^y \tau_j^y) + J_z \tau_i^z \tau_j^z \right] - 2B \sum_i \tau_i^z, \quad (6)$$

where we find that the two exchange anisotropies are now renormalized by the magnetoelastic interaction as

$$J_{xy} = -\frac{J^2}{D} - 2J\eta + \frac{(J\eta\Delta)^2}{D}, \quad (7a)$$

$$J_z = \frac{J^2}{D} + 4J\Delta - 2J\eta + \frac{(J\eta\Delta)^2}{D}. \quad (7b)$$

The quadrupolar nature of the Hamiltonian (6) becomes explicit, as the in-plane terms can be recast as

$$J_{xy} (\tau_i^x \tau_j^x + \tau_i^y \tau_j^y) = \frac{J_{xy}}{4} P (Q_i^{x^2-y^2} Q_j^{x^2-y^2} + Q_i^{xy} Q_j^{xy}) P. \quad (8)$$

Here, the on-site spin quadrupolar orders are defined as $Q_i^{x^2-y^2} = (S_i^x)^2 - (S_i^y)^2$ and $Q_i^{xy} = S_i^x S_i^y + S_i^y S_i^x$, which satisfy the relations $PQ_i^{x^2-y^2}P = 2\tau_x$ and $PQ_i^{xy}P = 2\tau_y$. A quadrupolar order $\langle Q \rangle$ in the original spin-1 model (2) is then translated to the dipole order $\langle \tau \rangle$ in the pseudospin-1/2 model (6). The quadrupolar order originates from the two-magnon processes (S^+S^+ and S^-S^-) that connect the local ground states $|S_z = +1\rangle$ and $|S_z = -1\rangle$. From Eq. (7), we find that J_{xy} and J_z share the same critical value $\eta_c = D/J\Delta^2$, below which ($0 < \eta < \eta_c$), increasing η results in an increase in $|J_{xy}|$ and a decrease in $|J_z|$. Specifically, a finite η can greatly enhance $|J_{xy}|$ while only moderately suppressing $|J_z|$. This asymmetry arises because the bare terms (at $\eta = 0$) are of second and first order in the pairwise exchange J for J_{xy} and J_z , respectively. Consequently, a physically accessible spin-lattice coupling ($\eta < 1 < \eta_c$) is expected to enhance the stability of the quadrupolar order by boosting the ratio $|J_{xy}/J_z|$. To justify this, we solve for the full phase diagram that is depicted in Fig. 1. We use the site-factorized $SU(2)$ coherent

state representation to minimize the energy of the effective Hamiltonian (6). Such a semiclassical method has captured all the phases calculated by density matrix renormalization group and infinite projected entangled pair states, with only a slight shift of the critical fields [5, 37].

The phase diagram is shown in Fig. 1, where four distinct phases, spin-nematic-supersolid (SNS), up-up-down (UUD), spin-nematic (SN) and fully polarized (FP) phases, are obtained. For the SN and FP phases, the ordering wavevector is at Γ . For both SNS and UUD phases, the ordering wavevector is at K and the magnetic unit cell has three sublattices (see Fig. 1). Up to a global rotation in the xy plane (Hamiltonian (6) has $U(1)$ symmetry), the directions of the effective spins τ_α for different phases are found to be

$$\text{SNS} : \hat{\tau}_A = \hat{\tau}_B = (\sin \theta_1, 0, \cos \theta_1), \quad \hat{\tau}_C = (\sin \theta_2, 0, \cos \theta_2), \quad (9a)$$

$$\text{UUD} : \hat{\tau}_A = \hat{\tau}_B = (0, 0, 1), \quad \hat{\tau}_C = (0, 0, -1), \quad (9b)$$

$$\text{SN} : \hat{\tau}_A = \hat{\tau}_B = \hat{\tau}_C = (\sin \phi, 0, \cos \phi), \quad (9c)$$

$$\text{FP} : \hat{\tau}_A = \hat{\tau}_B = \hat{\tau}_C = (0, 0, 1). \quad (9d)$$

Here, the angles θ_1 , θ_2 and ϕ are determined by minimizing the ground state energy [27]. In contrast to the SN phase, the SNS phase breaks the lattice translation symmetry of the original triangular lattice in a characteristic $\sqrt{3} \times \sqrt{3}$ pattern [38].

In Fig. 1, the regions for the SNS and SN phases are quite narrow at $\eta = 0$ [5], since $J_{xy}(\eta = 0) = J^2/D$ only has the high-order contribution from the bilinear pair-wise exchange term of Eq. (5). In the parameter choice of Fig. 1, the three critical fields at $\eta = 0$ are $B_{c,1}/J \approx 0.2$, $B_{c,2}/J = 7.52$, $B_{c,3}/J = 7.95$. In the low-field regime ($B < B_{c,1}$), the system stabilizes in the SNS state. Upon entering the intermediate field range ($B_{c,1} < B < B_{c,2}$), it exhibits UUD spin order. As B increases further ($B_{c,2} < B < B_{c,3}$), the system transitions into the SN phase. Finally, above the saturation field ($B > B_{c,3}$), the spins become fully polarized (FP phase). When η increases, $B_{c,1}$ shifts to higher values and $B_{c,2}$ decreases, whereas $B_{c,3}$ remains essentially unchanged (independent of η). Consequently, a finite η substantially enlarges the phase regions of both the SNS and SN states, allowing them to persist over a much broader range of magnetic fields as shown in Fig. 1. For a sufficiently large $\eta \gtrsim 0.9$, the SNS phase is no longer stable and will be overtaken by the SN phase. An order-of-magnitude estimation for η is left in supplementary material (SM) [27]. In both dipole-ordered phases (UUD and FP), the quadrupolar order parameter $|Q|$ vanishes identically, whereas $|Q|$ is finite only in the SNS and SN phases. Current experimental techniques, however, are primarily sensitive to the spin dipolar order $\langle S \rangle$, and cannot directly detect the quadrupolar order $|Q|$. Therefore, we next examine how the quadrupolar order of the SNS and SN phases affect the phonon spectra, leading to the practical route for phononic detection of hidden spin nematicity.

Spin-nematic phase.—To investigate the phonon spectrum with finite quadrupolar order in the SN phase, we start from the total Hamiltonian $H = H_s + H_p + H_{me}$ without integrating out the phonon fields, which can be written in the Nambu basis $\psi = (b_{1,\mathbf{k}}, b_{2,\mathbf{k}}, b_{1,-\mathbf{k}}^\dagger, b_{2,-\mathbf{k}}^\dagger, a_{\mathbf{k}}, a_{-\mathbf{k}}^\dagger)^T$ as

$H = \frac{1}{2} \sum_{\mathbf{k}} \psi^\dagger \mathcal{H}^{SN} \psi$. The creation operators for phonon and magnon are denoted by b^\dagger and a^\dagger , respectively. The kernel \mathcal{H}^{SN} takes a block matrix form [27]

$$\mathcal{H}^{SN} = \begin{pmatrix} \mathcal{H}_p(\mathbf{k}) & \Pi^\dagger(\mathbf{k}) \\ \Pi(\mathbf{k}) & \mathcal{H}_s(\mathbf{k}) \end{pmatrix}, \quad (10)$$

where \mathcal{H}_p and \mathcal{H}_s are the kernels for free phonon and magnon, respectively. $\Pi(\mathbf{k})$ originates from H_{me} [27]. By transforming the Hamiltonian $\mathcal{H}_{p-h}^{SN} = (\Lambda^{-1})^\dagger \mathcal{H}^{SN} \Lambda^{-1}$ to the particle-hole symmetric basis $\Psi = \Lambda \psi = (b_{1,\mathbf{k}}, b_{2,\mathbf{k}}, a_{\mathbf{k}}, b_{1,-\mathbf{k}}^\dagger, b_{2,-\mathbf{k}}^\dagger, a_{-\mathbf{k}}^\dagger)^T$, the diagonalization of the Hamiltonian $Q^\dagger \mathcal{H}_{p-h}^{SN} Q = \varepsilon$ can be mapped to a generalized eigenvalue problem $\mathcal{H}_{p-h}^{SN} Q = gQ\bar{\varepsilon}$ with the diagonal energy matrix $\bar{\varepsilon} \equiv g\varepsilon$ and metric $g = \sigma_z \otimes I_{3 \times 3}$. Here the Bogoliubov transformation Q must satisfy the condition $Q^\dagger g Q = QgQ^\dagger = g$ to maintain the correct bosonic commutation relation for magnon and phonon operators.

By writing the Hamiltonian in a quadratic form (10), we have required the dangling (linear) terms in H_s to vanish identically, whose presence indicates an unstable magnetic ground state. This condition yields two solutions for ϕ in Eq. (9c). The trivial solution $\phi = 0$ corresponds to the FP phase. The nontrivial solution $\phi = \arccos[2BD/3J^2(2 + \frac{4\Delta D}{J})]$ with lower energy corresponds to the SN phase. The spin configuration defined by this nontrivial solution exactly matches with the one obtained by minimizing energy in the SN phase at $\eta = 0$. The existence of this non-trivial solution imposes an upper bound of the magnetic field $B_{max} = 3J^2(2 + \frac{4\Delta D}{J})/2D$ for the SN phase, which is found to coincide with the upper boundary $B_{c,3} = B_{max}$ in Fig. 1.

In the SN phase with a monoatomic 2D unit cell, the spectrum comprises one magnon band and two low-energy acoustic phonon bands (no optical modes). The calculated energy spectra of Hamiltonian (10) are presented in Fig. 2 with a low intrinsic frequency for the acoustic phonon. In the first column ($\eta = 0$) of Fig. 2, the magnon dispersion is situated between the two phonon branches. The gapless feature of magnon bands (red line) is consistent with the spontaneous $U(1)$ symmetry breaking due to the finite in-plane dipole order $\langle \tau \rangle$.

In the presence of finite magnon-phonon coupling ($\eta \neq 0$), an avoided band gap opens at the energy crossings between the magnon and phonon bands as shown in the second column of Fig. 2. Several key features are worth noting. First, a finite η does not lift the degeneracy of phonon bands at the Γ and K points, as the magnetoelastic interaction H_{me} vanishes identically at these high-symmetry points. Second, although there are multiple crossings between the magnon and phonon bands, only one avoided crossing emerges prominently. Third, the position of this gap is very sensitive to the magnetic field. As we gradually increase the magnetic field, the position of the avoided crossing sweeps through the K point. Since the gap is enforced to close exactly at K (due to vanishing H_{me}), we expect the magnitude of this avoided crossing, denoted as Δ_a , to exhibit a non-monotonic dependence on the magnetic field. In Fig. 3, we plot Δ_a as a function of magnetic field

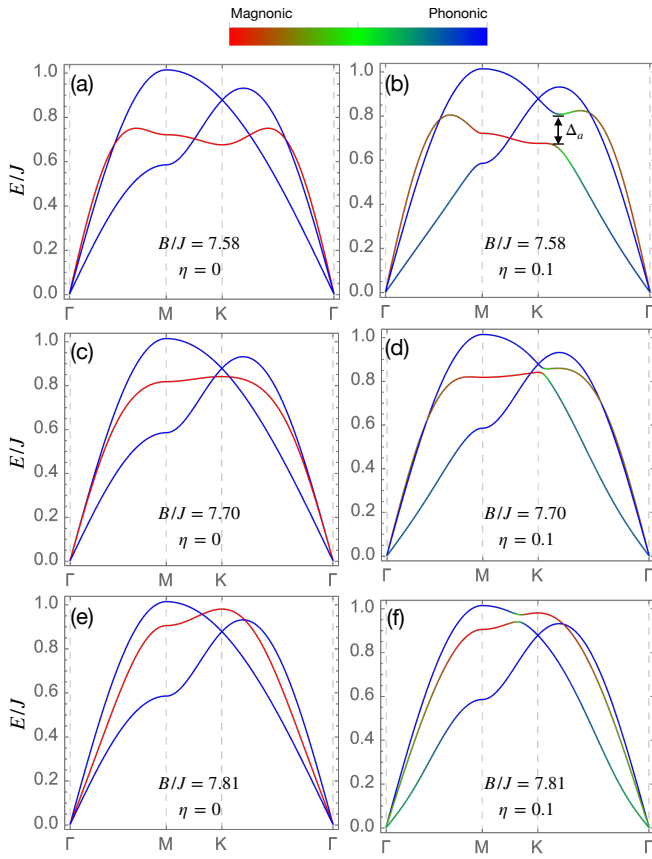


FIG. 2. Phonon–magnon band spectra in SN phase under different magnetic fields in the absence [(a), (c), and (e)] and presence [(b), (d), and (f)] of magnon–phonon coupling. The color represents the normalized relative weight of the phonon-like and magnon-like components of each band. The intrinsic frequency $\hbar\omega_0/J = 0.41$.

for various coupling strengths η . It is clear that Δ_a increases with increasing η . Most importantly, there exists a critical magnetic field where the crossing position can be tuned to be right at the K point, yielding a vanishing gap $\Delta_a(K) = 0$ (Fig. 3). Tuning the magnetic field away from this critical point reopens an observable gap. Consequently, Δ_a demonstrates a non-monotonic dependence on B , as anticipated. All the non-trivial features of the phonon bands discussed above serve as a distinct signature for probing the SN phase.

Spin-nematic-supersolid phase.—In the SNS phase, the unit cell contains three sublattices (Fig. 1). Thus, we enlarge the unit cell for phonons to include the magnon-phonon coupling. We obtain six phonon bands in total and four of them are the fictitious optical modes due to the band folding, which can be projected out by the projector P^{ac} constructed specifically for the acoustic modes [27].

Following the same procedure as in the SN phase, we find that the vanishing of dangling (linear) terms in H_s yields two transcendental equations for the angle θ_1 and θ_2 [27]. The trivial solution $\theta_1 = 0, \theta_2 = \pi$ corresponds to the UUD phase while the nontrivial solution corresponds to the SNS phase, which exactly matches the one obtained from minimizing the

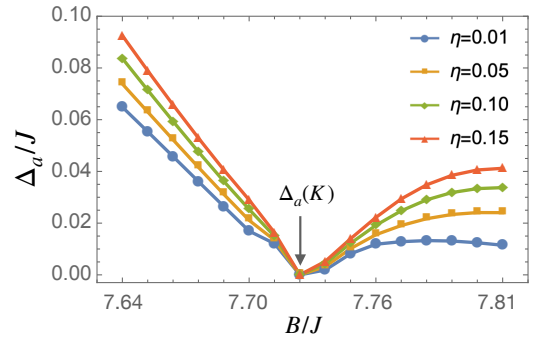


FIG. 3. Magnitude of the avoided crossing gap Δ_a as a function of magnetic field in the SN phase. The black arrow indicates the critical magnetic field $B/J \approx 7.72$ where Δ_a vanishes at the K point.

energy in the SNS phase. Again, the existence of such non-trivial solution imposes an upper bound B_{max} of the magnetic field for the SNS phase, which coincides with the threshold $B_{max} = B_{c,1}$ of Fig. 1(b). After obtaining a stable magnetic ground state, we plot the phonon and magnon band spectra for different magnetic fields in Fig. 4.

In stark contrast to the SN phase where the gap opens at a single crossing point, the SNS phase exhibits multiple avoided band gaps across the spectrum. This complexity arises because H_s and H_{me} highly depend on the underlying spin order and the magnetoelastic interaction in the SNS phase allows richer couplings. The color-coded spectral weights in Figs. 4(b) and (e) reveal strong hybridization at all the crossings between magnons and phonons. With increasing magnetic field, the avoided band gaps shift to higher energy. The hybridization between magnons and fictitious optical phonons occurs around the M and K points in the middle of the energy spectra. The two low-energy phonon bands at the K point originate from band folding associated with the enlarged unit cell adopted for the phonon. In Figs. 4(c) and (f), we show the band spectra where such fictitious optical bands are removed by the projector P^{ac} . Importantly, the magnon band can display splittings even in regions devoid of genuine acoustic phonon modes [Figs. 4(c) and (f)]. Physically, these gaps originate from the interaction between magnons and the folded phonon branches (Umklapp scattering). The degeneracies of phonon bands at K and Γ points cannot be lifted by a finite η .

In Fig. 4, only two magnon bands are shown, while a high-energy flat band (around $E/J \sim 14.5$), which is insensitive to the magnetic field, is not explicitly displayed. The emergence of this high-energy flat band can be attributed to the geometrical frustration of the triangular lattice in the $J_z \gg J_{xy}$ Ising limit [39]. We find that this flat band is completely decoupled from the lattice degrees of freedom, even when the phonon energies are artificially increased to force energy crossings for the magnon flat band, a finite ($\eta \neq 0$) fails to open any spectral gap.

Discussion.—We conclude that the spin–lattice coupling plays two key roles in our work. First, it substantially enhances the stability of the SN and SNS phases. Second, it

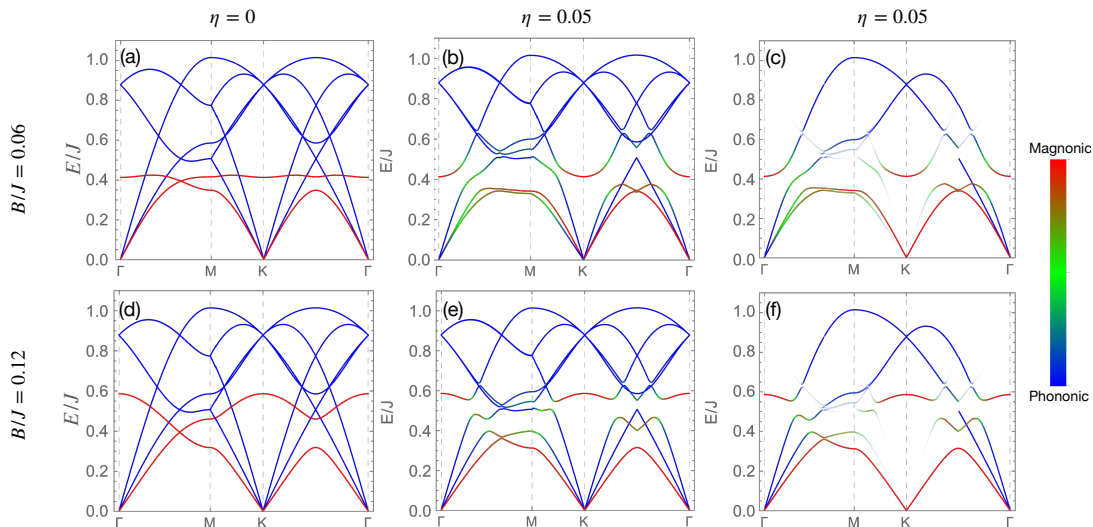


FIG. 4. Phonon–magnon band spectra in SNS phase with magnetic field $B/J = 0.06$ [first row, (a-c)] and $B/J = 0.12$ [second row, (d-f)]. In the first column [(a) and (d)], the magnon-phonon coupling is turned off ($\eta = 0$). In the second column [(b) and (e)], the magnon-phonon coupling is turned on ($\eta \neq 0$). (c) and (f) are the same as (b) and (e) but with the fictitious optical modes projected out. The intrinsic frequency ω_0 takes the same value as in Fig. 2.

induces avoided crossings in the phonon spectrum that depend on the underlying spin ground state, enabling a practical phononic probe of the otherwise hidden quadrupolar order. The implications of successfully detecting spin nematicity via phonons are profound and open several new research avenues. Our methodology could be generalized to probe other elusive forms of hidden orders, such as those found in spin liquids [40, 41] or other multipolar states [35, 42], across different lattice geometries. Furthermore, studying the interplay between phonons and the dynamical quadrupolar structure factor could yield fresh insights into the low-energy excitations of the multipolar order [43, 44].

Beyond the solid-state systems, these concepts could be tested in tunable quantum simulator platforms, such as spin-1 Bose-Einstein condensates [23], where spin-spin correlations can be engineered and observed with high precision. Thus, leveraging the bond phonon model not only solves an immediate detection problem but also establishes a versatile new paradigm for exploring the rich landscape of complex quantum magnetism. Recently, we became aware of related work [45] that employs on-site (Einstein) phonons to probe spin-orbit-entangled multipolar order through the lifting of the E_g -doublet degeneracy; by contrast, our bond-phonon mechanism can both enhance and diagnose a purely-spin quadrupolar order via robust magnon-phonon hybridization (avoided crossings), without lifting the phonon degeneracies.

Acknowledgments.—We thank Jiahao Yang for the fruitful discussions. This work is supported by NSFC No.92565110, No.12574061, and by the Ministry of Science and Technology of China with Grants No. 2021YFA1400300.

* chenxray@pku.edu.cn

- [1] K. Penc and A. M. Läuchli, Spin nematic phases in quantum spin systems, in *Introduction to Frustrated Magnetism: Materials, Experiments, Theory*, edited by C. Lacroix, P. Mendels, and F. Mila (Springer Berlin Heidelberg, Berlin, Heidelberg, 2011) pp. 331–362.
- [2] L. V. Pourovskii, D. Fiore Mosca, L. Celiberti, S. Khmelevskiy, A. Paramekanti, and C. Franchini, Hidden orders in spin–orbit-entangled correlated insulators, *Nature Reviews Materials* **10**, 674 (2025).
- [3] H. Tsunetsugu and M. Arikawa, Spin Nematic Phase in S=1 Triangular Antiferromagnets, *Journal of the Physical Society of Japan* **75**, 083701 (2006).
- [4] N. Papanicolaou, Unusual phases in quantum spin-1 systems, *Nuclear Physics B* **305**, 367 (1988).
- [5] J. Sheng, J. Hu, L. Xu, L. Wang, X. Shi, R. Chi, D. Yu, A. Podlesnyak, P. Piyawongwathana, N. Murai, S. Ohira-Kawamura, H. Yuan, L. Wang, J.-W. Mei, H.-J. Liao, T. Xiang, L. Wu, and Z. Wang, Possible Observation of Quadrupole Waves in Spin Nematics, *Phys. Rev. Lett.* **135**, 156704 (2025).
- [6] S. Bhattacharjee, V. B. Shenoy, and T. Senthil, Possible ferro-spin nematic order in NiGa_2S_4 , *Phys. Rev. B* **74**, 092406 (2006).
- [7] O. A. Starykh, Unusual ordered phases of highly frustrated magnets: a review, *Reports on Progress in Physics* **78**, 052502 (2015).
- [8] P. Chandra and P. Coleman, Quantum spin nematics: Moment-free magnetism, *Phys. Rev. Lett.* **66**, 100 (1991).
- [9] A. Smerald and N. Shannon, Theory of spin excitations in a quantum spin-nematic state, *Phys. Rev. B* **88**, 184430 (2013).
- [10] Y. Huang, S. Yunoki, and S. Maekawa, *Emergent spin supersolids in frustrated quantum materials* (2026).
- [11] D. Podolsky and E. Demler, Properties and detection of spin nematic order in strongly correlated electron systems, *New Journal of Physics* **7**, 59 (2005).

- [12] Y. Kohama, H. Ishikawa, A. Matsuo, K. Kindo, N. Shannon, and Z. Hiroi, Possible observation of quantum spin-nematic phase in a frustrated magnet, *Proceedings of the National Academy of Sciences* **116**, 10686 (2019).
- [13] H. Kim, J.-K. Kim, J. Kwon, J. Kim, H.-W. J. Kim, S. Ha, K. Kim, W. Lee, J. Kim, G. Y. Cho, H. Heo, J. Jang, C. J. Sahle, A. Longo, J. Stremper, G. Fabbri, Y. Choi, D. Haskel, J. Kim, J.-W. Kim, and B. J. Kim, Quantum spin nematic phase in a square-lattice iridate, *Nature* **625**, 264 (2024).
- [14] O. Halpern and M. H. Johnson, On the magnetic scattering of neutrons, *Phys. Rev.* **55**, 898 (1939).
- [15] B. N. Brockhouse, Scattering of neutrons by spin waves in magnetite, *Phys. Rev.* **106**, 859 (1957).
- [16] J. Cui, E. V. Boström, M. Ozerov, F. Wu, Q. Jiang, J.-H. Chu, C. Li, F. Liu, X. Xu, A. Rubio, and Q. Zhang, Chirality selective magnon-phonon hybridization and magnon-induced chiral phonons in a layered zigzag antiferromagnet, *Nature Communications* **14**, 3396 (2023).
- [17] R. Loudon, The raman effect in crystals, *Advances in Physics* **13**, 423 (1964).
- [18] E. Burkel, J. Peisl, and B. Dorner, Observation of inelastic x-ray scattering from phonons, *Europhysics Letters* **3**, 957 (1987).
- [19] M. Krisch and F. Sette, Inelastic x-ray scattering from phonons, in *Light Scattering in Solid IX*, edited by M. Cardona and R. Merlin (Springer Berlin Heidelberg, Berlin, Heidelberg, 2007) pp. 317–370.
- [20] R. Silbergliitt and J. B. Torrance, Effect of Single-Ion Anisotropy on Two-Spin-Wave Bound State in a Heisenberg Ferromagnet, *Phys. Rev. B* **2**, 772 (1970).
- [21] T. Oguchi, Theory of two-magnon bound states in the heisenberg ferro- and antiferromagnet, *Journal of the Physical Society of Japan* **31**, 394 (1971).
- [22] X. Bai, S.-S. Zhang, Z. Dun, H. Zhang, Q. Huang, H. Zhou, M. B. Stone, A. I. Kolesnikov, F. Ye, C. D. Batista, and M. Mourigal, Hybridized quadrupolar excitations in the spin-anisotropic frustrated magnet FeI_2 , *Nature Physics* **17**, 467 (2021).
- [23] J. Sheng, J.-W. Mei, L. Wang, X. Xu, W. Jiang, L. Xu, H. Ge, N. Zhao, T. Li, A. Candini, B. Xi, J. Zhao, Y. Fu, J. Yang, Y. Zhang, G. Biasiol, S. Wang, J. Zhu, P. Miao, X. Tong, D. Yu, R. Mole, Y. Cui, L. Ma, Z. Zhang, Z. Ouyang, W. Tong, A. Podlesnyak, L. Wang, F. Ye, D. Yu, W. Yu, L. Wu, and Z. Wang, Bose–Einstein condensation of a two-magnon bound state in a spin-1 triangular lattice, *Nature Materials* **24**, 544 (2025).
- [24] These two methods are complementary limits of the same magnetoelastic model. In the spin-only treatment, the phonons are integrated out, which captures their static backaction on the spin sector and is used to determine the static spin phase diagram. In the spectral calculation, the phonon degrees of freedom are retained explicitly so that their dynamical (finite- k) hybridization with magnons can be resolved and used as a spectroscopic probe of hidden spin nematicity.
- [25] D. L. Bergman, R. Shindou, G. A. Fiete, and L. Balents, Models of degeneracy breaking in pyrochlore antiferromagnets, *Phys. Rev. B* **74**, 134409 (2006).
- [26] S. Streib, N. Vidal-Silva, K. Shen, and G. E. W. Bauer, Magnon-phonon interactions in magnetic insulators, *Phys. Rev. B* **99**, 184442 (2019).
- [27] See supplemental material at [URL will be inserted by publisher] for the details of the effective Hamiltonian and projection operators.
- [28] M. Blume and Y. Y. Hsieh, Biquadratic exchange and quadrupolar ordering, *Journal of Applied Physics* **40**, 1249 (1969).
- [29] A. Läuchli, F. Mila, and K. Penc, Quadrupolar phases of the $s = 1$ bilinear-biquadratic heisenberg model on the triangular lattice, *Phys. Rev. Lett.* **97**, 087205 (2006).
- [30] M. Moreno-Cardoner, H. Perrin, S. Paganelli, G. De Chiara, and A. Sanpera, Case study of the uniaxial anisotropic spin-1 bilinear-biquadratic heisenberg model on a triangular lattice, *Phys. Rev. B* **90**, 144409 (2014).
- [31] K. Tanaka, Y. Yokoyama, and C. Hotta, Origin of biquadratic exchange interactions in a mott insulator as a driving force of spin nematic order, *Journal of the Physical Society of Japan* **87**, 023702 (2018).
- [32] S. Hayami, R. Ozawa, and Y. Motome, Effective bilinear-biquadratic model for noncoplanar ordering in itinerant magnets, *Phys. Rev. B* **95**, 224424 (2017).
- [33] Y. Akagi, M. Udagawa, and Y. Motome, Hidden multiple-spin interactions as an origin of spin scalar chiral order in frustrated kondo lattice models, *Phys. Rev. Lett.* **108**, 096401 (2012).
- [34] J. G. Rau, S. Petit, and M. J. P. Gingras, Order by virtual crystal field fluctuations in pyrochlore XY antiferromagnets, *Phys. Rev. B* **93**, 184408 (2016).
- [35] P. Santini, S. Carretta, G. Amoretti, R. Caciuffo, N. Magnani, and G. H. Lander, Multipolar interactions in f -electron systems: The paradigm of actinide dioxides, *Rev. Mod. Phys.* **81**, 807 (2009).
- [36] O. Tchernyshyov, R. Moessner, and S. L. Sondhi, Order by distortion and string modes in pyrochlore antiferromagnets, *Phys. Rev. Lett.* **88**, 067203 (2002).
- [37] D. Yamamoto, G. Marmorini, and I. Danshita, Quantum Phase Diagram of the Triangular-Lattice XXZ Model in a Magnetic Field, *Phys. Rev. Lett.* **112**, 127203 (2014).
- [38] D. Heidarian and K. Damle, Persistent supersolid phase of hard-core bosons on the triangular lattice, *Phys. Rev. Lett.* **95**, 127206 (2005).
- [39] G. H. Wannier, Antiferromagnetism. The Triangular Ising Net, *Phys. Rev.* **79**, 357 (1950).
- [40] X.-G. Wen, Quantum orders and symmetric spin liquids, *Phys. Rev. B* **65**, 165113 (2002).
- [41] Y. Zhou, K. Kanoda, and T.-K. Ng, Quantum spin liquid states, *Rev. Mod. Phys.* **89**, 025003 (2017).
- [42] A. S. Patri, A. Sakai, S. Lee, A. Paramekanti, S. Nakatsuji, and Y. B. Kim, Unveiling hidden multipolar orders with magnetostriction, *Nature Communications* **10**, 4092 (2019).
- [43] B.-Q. Liu, P. Čermák, C. Franz, C. Pfeleiderer, and A. Schneidewind, Lattice dynamics and coupled quadrupole-phonon excitations in CeAuAl_3 , *Phys. Rev. B* **98**, 174306 (2018).
- [44] K. Hart, R. Sutcliffe, G. Refael, and A. Paramekanti, *Phonon-driven multipolar dynamics in a spin-orbit coupled mott insulator* (2025).
- [45] R. Sutcliffe, K. Hart, S. Chaudhary, and A. Paramekanti, *Pseudo-chiral phonon splitting from octupolar magnetic order* (2025), [arXiv:2506.18978 \[cond-mat.str-el\]](https://arxiv.org/abs/2506.18978).
- [46] T. Holstein and H. Primakoff, Field dependence of the intrinsic domain magnetization of a ferromagnet, *Phys. Rev.* **58**, 1098 (1940).
- [47] M. Vogl, P. Laurell, H. Zhang, S. Okamoto, and G. A. Fiete, Resummation of the holstein-primakoff expansion and differential equation approach to operator square roots, *Phys. Rev. Res.* **2**, 043243 (2020).

Supplementary material for “Phononic enhancement and detection of hidden spin-nematicity and dynamics in quantum magnets”

Junyu Tang¹, Hong-Hao Song¹, Gang v. Chen^{1,2}

¹*International Center for Quantum Materials, School of Physics, Peking University, Beijing 100871, China*

²*Collaborative Innovation Center of Quantum Matter, 100871, Beijing, China*

Schrieffer–Wolff transformation	7
Effective spin Hamiltonian	8
Estimation for η	9
Spin-nematic phase	10
Spin-nematic-supersolid phase	12
Projection operators	14

SCHRIEFFER–WOLFF TRANSFORMATION

The spin-1 XXZ Hamiltonian [Eq.(2) of main text] can be divided into as $H = H_0 + V$, where the perturbation $V = J \sum_{\langle i,j \rangle} (S_i^x S_j^x + S_i^y S_j^y) = J \sum_{\langle i,j \rangle} (S_i^+ S_j^- + S_i^- S_j^+)/2$ corresponds to the spin flipping and thus belongs the high energy part ($D \gg J, g_c \mu_B B$). The Schrieffer–Wolff transformation seeks for a transformation $H' = e^S H e^{-S} = H_0 + \frac{1}{2}[S, V] + O(V^3)$ that projects into the effective low-energy space. The generator S should satisfy the condition $V + [S, H_0] = 0$. Most importantly, H_0 is diagonal while the perturbation is purely off-diagonal ($V_{nn} = 0$) in the low-energy space. Therefore, we have the following solution for the generator S :

$$\frac{1}{2}[S, V]_{mn} = \frac{1}{2} \sum_k V_{mk} V_{kn} \left[\frac{1}{E_m - E_k} - \frac{1}{E_k - E_n} \right], \quad (\text{S1})$$

where $O_{nm} \equiv \langle n | \hat{O} | m \rangle$ and E_n is the energy of state $|n\rangle$. After plugging the expression of V into above equation, we find the following four terms for $V_{mk} V_{kn}$

$$\begin{aligned} V_{mk} V_{kn} = & \frac{J^2}{4} \langle m | S_i^+ S_j^- | k \rangle \langle k | S_i^+ S_j^- | n \rangle + \frac{J^2}{4} \langle m | S_i^- S_j^+ | k \rangle \langle k | S_i^- S_j^+ | n \rangle \\ & + \frac{J^2}{4} \langle m | S_i^+ S_j^- | k \rangle \langle k | S_i^- S_j^+ | n \rangle + \frac{J^2}{4} \langle m | S_i^- S_j^+ | k \rangle \langle k | S_i^+ S_j^- | n \rangle \end{aligned} \quad (\text{S2})$$

If we denote the state at site i, j as

$$|S_i^z, S_j^z\rangle \equiv |S_i^z\rangle |S_j^z\rangle, \quad S_z = \pm 1 \rightarrow \{1, \bar{1}\}$$

, then it's easy to see that the first term only has a contribution from $|m\rangle = |1, \bar{1}\rangle, |k\rangle = |0, 0\rangle, |n\rangle = |\bar{1}, 1\rangle$. Similarly, the second term only has a contribution from $|m\rangle = |\bar{1}, 1\rangle, |k\rangle = |0, 0\rangle, |n\rangle = |1, \bar{1}\rangle$. Combining with Eq. (S1), the first two terms of Eq. (S2) yield a Hamiltonian containing $-\frac{J^2}{2D} |1, \bar{1}\rangle \langle \bar{1}, 1|$ and $-\frac{J^2}{2D} |\bar{1}, 1\rangle \langle 1, \bar{1}|$, which corresponds to a biquadratic Hamiltonian

$$-\frac{J^2}{8D} \sum_{\langle i,j \rangle} (S_i^+ S_i^+ S_j^- S_j^- + S_i^- S_i^- S_j^+ S_j^+) \quad (\text{S3})$$

The last two terms of Eq. (S2) need a careful examination, where we find that a nonvanishing contribution requires $|m\rangle = |n\rangle$. However, among the four possible states of $|m\rangle$ and $|n\rangle$ for $\langle m | S_i^+ S_j^- | k \rangle \langle k | S_i^- S_j^+ | n \rangle$, only $|n\rangle = |1, \bar{1}\rangle, |m\rangle = |\bar{1}, 1\rangle$ are relevant to us since they reside in the desired low energy space, which is connected through an intermediate high-energy virtual state

$|k\rangle = |0,0\rangle$. Similarly, for $\langle m|S_i^- S_j^+ |k\rangle \langle k|S_i^+ S_j^- |n\rangle$, we only has the contribution from $|n\rangle = |\bar{1}, 1\rangle, |k\rangle = |0,0\rangle, |m\rangle = |\bar{1}, 1\rangle$. Combining with Eq. (S1), the last two terms of Eq. (S2) yield a Hamiltonian containing $-\frac{J^2}{2D}|1, \bar{1}\rangle \langle 1, \bar{1}|$ and $-\frac{J^2}{2D}|\bar{1}, 1\rangle \langle \bar{1}, 1|$, which corresponds to the operator $\frac{J^2}{4D}S_i^z S_j^z$ plus some constant coefficient proportional to the identity operator that can be neglected.

To conclude, after performing the Schrieffer–Wolff transformation, The bilinear term $J\sum_{\langle i,j\rangle}(S_i^+ S_j^- + S_i^- S_j^+)/2$ in H_s contributes to a Hamiltonian in the form of

$$-\frac{J^2}{8D}\sum_{\langle i,j\rangle}(S_i^+ S_i^+ S_j^- S_j^- + S_i^- S_i^- S_j^+ S_j^+) + \frac{J^2}{4D}S_i^z S_j^z \quad (\text{S4})$$

In the next section, we will see how phonon affects the coefficient of the bilinear term and meanwhile brings the additional biquadratic term.

EFFECTIVE SPIN HAMILTONIAN

The phonon field \mathbf{u}_{ij} enters the Hamiltonian quadratically in H_p and linearly in H_{me} . Additionally, each \mathbf{u}_{ij} couples only to a single nearest-neighbor pair of spins, and can be treated as an independent variable[25]. Consequently, the phonon field can be eliminated analytically by a Gaussian integration:

$$e^{-\beta H_s^{\text{eff}}} = \prod_{\langle i,j\rangle} \int \mathcal{D}\mathbf{u}_{ij} e^{-\beta(H_s + H_p[\mathbf{u}_{ij}] + H_{me}[\mathbf{u}_{ij}])}, \quad (\text{S5})$$

where $\beta = 1/k_B T$. We note that completing the square in the exponent is physically equivalent to replacing the \mathbf{u}_{ij} field with the equilibrium value that minimizes the total energy $H_p[\mathbf{u}_{ij}] + H_{me}[\mathbf{u}_{ij}]$. Thus, up to a constant term, one obtains

$$H_s^{\text{eff}} = H_s - J\eta \sum_{\langle i,j\rangle} (S_i^x S_j^x + S_i^y S_j^y + \Delta S_i^z S_j^z)^2, \quad (\text{S6})$$

which is Eq.(5) in the main text. Notably, the biquadratic term emerges in the effective Hamiltonian after integrating out the phonon field. Expanding the square of this biquadratic term, we find

$$\begin{aligned} -J\eta \sum_{\langle i,j\rangle} (S_i^x S_j^x + S_i^y S_j^y + \Delta S_i^z S_j^z)^2 &= -\frac{J\eta}{4} \sum_{\langle i,j\rangle} (S_i^+ S_j^- + S_i^- S_j^+)^2 + 2\Delta S_i^z S_j^z (S_i^+ S_j^- + S_i^- S_j^+) + 2\Delta (S_i^+ S_j^- + S_i^- S_j^+) S_i^z S_j^z \\ &= -\frac{J\eta}{4} \sum_{\langle i,j\rangle} (S_i^+ S_i^+ S_j^- S_j^- + S_i^- S_i^- S_j^+ S_j^+ + S_i^+ S_i^- S_j^- S_j^+ + S_i^- S_i^+ S_j^+ S_j^-) \\ &\quad - J\eta\Delta \sum_{\langle i,j\rangle} S_i^z S_j^z \frac{(S_i^+ S_j^- + S_i^- S_j^+)}{2} - J\eta\Delta \sum_{\langle i,j\rangle} \frac{(S_i^+ S_j^- + S_i^- S_j^+)}{2} S_i^z S_j^z \end{aligned} \quad (\text{S7})$$

where we have ignore the term $\Delta^2 (S_i^z)^2 (S_j^z)^2$, which corresponds to a constant term in the low-energy space. The effective spin Hamiltonian now becomes

$$\begin{aligned} H_s^{\text{eff}} &= J \sum_{\langle i,j\rangle} \left[\frac{(1 - \eta\Delta S_i^z S_j^z)(S_i^+ S_j^- + S_i^- S_j^+) - (S_i^+ S_j^- + S_i^- S_j^+) \eta\Delta S_i^z S_j^z}{2} \right] \\ &\quad - \frac{J\eta}{4} \sum_{\langle i,j\rangle} (S_i^+ S_i^+ S_j^- S_j^- + S_i^- S_i^- S_j^+ S_j^+ + S_i^+ S_i^- S_j^- S_j^+ + S_i^- S_i^+ S_j^+ S_j^-) \\ &\quad + \sum_{\langle i,j\rangle} J\Delta S_i^z S_j^z - D \sum_i (S_i^z)^2 - g_c \mu_B B \sum_i S_i^z. \end{aligned} \quad (\text{S8})$$

We note that the first term (first line), which correspond to one-magnon process cannot survive from by the projection $P_i = |1_i\rangle \langle 1_i| + |\bar{1}_i\rangle \langle \bar{1}_i|$ for low-energy space ($P_i S_i^\pm P_i = 0$). Consequently, we perform the Schrieffer–Wolff transformation with perturbation $V = J[(1 - \eta\Delta S_i^z S_j^z)(S_i^+ S_j^- + S_i^- S_j^+) - (S_i^+ S_j^- + S_i^- S_j^+) \eta\Delta S_i^z S_j^z]/2$. In contrast to the previous section where V consisted of only two terms [$V = J(S_i^+ S_j^- + S_i^- S_j^+)/2$], here V contains six terms, leading to 36 possible contributions to the matrix element product $V_{mk} V_{kn}$. Fortunately, the four additional terms involve only S^z operator, which is diagonal in the spin basis (does

not change the spin state). Most importantly, many of these terms vanish because the S^z operator annihilates the only allowed intermediate virtual state $|k\rangle = |0, 0\rangle$, as demonstrated previously. Overall, we obtain the effective terms from the perturbation V as

$$-\frac{J^2(1-\eta^2\Delta^2)}{2D}|1, \bar{1}\rangle\langle\bar{1}, 1| - \frac{J^2(1-\eta^2\Delta^2)}{2D}|\bar{1}, 1\rangle\langle 1, \bar{1}| - \frac{J^2(1-\eta\Delta)^2}{2D}|1, \bar{1}\rangle\langle 1, \bar{1}| - \frac{J^2(1+\eta\Delta)^2}{2D}|\bar{1}, 1\rangle\langle\bar{1}, 1|, \quad (\text{S9})$$

where the first two terms can be easily mapped to the biquadratic term

$$-\frac{J^2}{8D}(1-\eta^2\Delta^2)(S_i^+S_i^+S_j^-S_j^- + S_i^-S_i^-S_j^+S_j^+). \quad (\text{S10})$$

The last two terms of Eq. (S9) need further careful examination. But since they only involve ket and bra states of the same spin state, we can solve the linear equation $C_0I_i \otimes I_j + C_1S_i^z \otimes S_j^z + C_2I_i \otimes S_j^z + C_3S_i^z \otimes I_j$ for the operators of the last two terms. The four coefficients are found to be

$$C_0 = -\frac{J^2(1+\eta^2\Delta^2)}{4D}, \quad C_1 = \frac{J^2(1+\eta^2\Delta^2)}{4D}, \quad C_2 = \frac{-J^2\eta\Delta}{2D}, \quad C_3 = \frac{J^2\eta\Delta}{2D} \quad (\text{S11})$$

Note that the C_0 term is just a constant term, which can be simply neglected. The C_2 and C_3 term correspond to a staggered Zeeman field induced by the phonon that couples to the S^z at site i and j . Nevertheless, after a summation for each bond of triangular lattice, they cancel out. Therefore, we only need the C_1 term. Collecting all the necessary terms, the effective spin Hamiltonian now becomes

$$\begin{aligned} H_s^{\text{eff}} = & -\left[\frac{J\eta}{4} + \frac{J^2}{8D}(1-\eta^2\Delta^2)\right] \sum_{\langle i,j \rangle} (S_i^+S_i^+S_j^-S_j^- + S_i^-S_i^-S_j^+S_j^+) - \frac{J\eta}{4} \sum_{\langle i,j \rangle} (S_i^+S_i^-S_j^-S_j^+ + S_i^-S_i^+S_j^+S_j^-) \\ & + \sum_{\langle i,j \rangle} \left[J\Delta + \frac{J^2(1+\eta^2\Delta^2)}{4D} \right] S_i^z S_j^z - D \sum_i (S_i^z)^2 - g_c \mu_B B \sum_i S_i^z. \end{aligned} \quad (\text{S12})$$

We can now directly apply the projection operator $P_i = |1_i\rangle\langle 1_i| + |\bar{1}_i\rangle\langle\bar{1}_i|$ to each spin site for the low-energy spin-1/2 space. It's easy to find the following mapping between the effective spin-1/2 space and original spin-1 space

$$\frac{1}{2}P_i S_i^z P_i = \frac{1}{2}(|1_i\rangle\langle 1_i| - |\bar{1}_i\rangle\langle\bar{1}_i|) = \frac{1}{2} \begin{pmatrix} 1 & 0 \\ 0 & -1 \end{pmatrix} = \tau_i^z \quad (\text{S13a})$$

$$\frac{1}{2}P_i S_i^+ S_i^+ P_i = |1_i\rangle\langle\bar{1}_i| = \begin{pmatrix} 0 & 1 \\ 0 & 0 \end{pmatrix} = \tau_i^+ = (\tau_i^x + i\tau_i^y) \quad (\text{S13b})$$

$$\frac{1}{2}P_i S_i^- S_i^- P_i = |\bar{1}_i\rangle\langle 1_i| = \begin{pmatrix} 0 & 0 \\ 1 & 0 \end{pmatrix} = \tau_i^- = (\tau_i^x - i\tau_i^y) \quad (\text{S13c})$$

$$\frac{1}{2}P_i S_i^+ S_i^- P_i = |1_i\rangle\langle 1_i| = \begin{pmatrix} 1 & 0 \\ 0 & 0 \end{pmatrix} = \tau_i^0 + \tau_i^z \quad (\text{S13d})$$

$$\frac{1}{2}P_i S_i^- S_i^+ P_i = |\bar{1}_i\rangle\langle\bar{1}_i| = \begin{pmatrix} 0 & 0 \\ 0 & 1 \end{pmatrix} = \tau_i^0 - \tau_i^z \quad (\text{S13e})$$

Then, the effective spin Hamiltonian takes the following final form:

$$H_s^{\text{eff}} = -\frac{J^2}{D} \sum_{\langle i,j \rangle} \left[\left(1 + \frac{2D\eta}{J} - \eta^2\Delta^2\right) (\tau_i^x \tau_j^x + \tau_i^y \tau_j^y) - \left(1 + \frac{2D(2\Delta - \eta)}{J} + \eta^2\Delta^2\right) \tau_i^z \tau_j^z \right] - 2g_c \mu_B B \sum_i \tau_i^z, \quad (\text{S14})$$

which corresponds to the Eq.(6) of the main text after the substitution $g_c \mu_B B \rightarrow B$ (which changes the unit of magnetic field from Tesla to the energy unit Joule).

ESTIMATION FOR η

Here, we discuss and present an order-of-magnitude estimation for η . The effective mass of the vibrating atom can be set to $M \simeq 60u \simeq 10^{-25}$ kg, which is representative of a $3d$ transition-metal ion. We adopt a low intrinsic vibration frequency

$\omega_0 \simeq 62.8$ GHz for the acoustic phonon. As for the exchange-length sensitivity, we take a conservative range $\gamma \simeq 0.1\text{--}0.5 \text{ \AA}^{-1}$. Putting these values together into the expression $\eta = J\gamma^2/k_E = J\gamma^2/M\omega_0^2$, we obtain

$$\eta \simeq 0.04\text{--}1 \quad (\gamma = 0.1\text{--}0.5 \text{ \AA}^{-1}). \quad (\text{S15})$$

It is worth noting that for a large ω_0 in the sub-THz range, η could be significantly suppressed to zero due to the $1/\omega_0^2$ factor in its expression. Furthermore, a large mismatch between magnon and phonon energy scales results in a scenario where mode crossings appear only in the immediate vicinity of the Γ point, rendering the phonon probe ineffective. While a large exchange J could address both the energy mismatch and the small η issues, it would necessitate an impractically large critical field for the SN phase. On the other hand, although a large γ could enhance η via the γ^2 factor in its expression, it fails to bridge the energy gap between magnons and phonons. Therefore, in our numerical calculations, we have adopted a compromise for the energy scales of low-energy acoustic phonon ($\omega_0 = 62.8$ GHz) and magnon ($\omega_m \equiv J/\hbar = 151.7$ GHz) to avoid further parameter tuning. In the phase diagram, the y axis is plotted up to the upper limit $\eta = 1$ to provide a comprehensive theoretical overview. We emphasize that, other choices of the ω_0, ω_m, η do not qualitatively change the conclusion and results of this work.

SPIN-NEMATIC PHASE

The free phonon Hamiltonian H_p after transforming to the reciprocal space reads

$$H_p = \frac{1}{2M} \sum_{\mathbf{k}} \vec{p}_{\mathbf{k}}^\dagger J \vec{p}_{\mathbf{k}} + \frac{1}{2} \sum_{\mathbf{k}} \vec{u}_{\mathbf{k}}^\dagger \mathcal{D}(\mathbf{k}) \vec{u}_{\mathbf{k}} \quad (\text{S16})$$

where $\vec{p}_{\mathbf{k}} = (p_{\mathbf{k}}^x, p_{\mathbf{k}}^y)^T$ and \mathcal{D} is the dynamical matrix in the basis $\vec{u}_{\mathbf{k}} = (u_{\mathbf{k}}^x, u_{\mathbf{k}}^y)^T$. The dynamical matrix \mathcal{D} of the phonon in the triangular lattice of the SN phase is simply a 2×2 matrix, which under the basis of $(u_{\mathbf{k}}^x, u_{-\mathbf{k}}^y)$ reads

$$\mathcal{D}(\mathbf{k}) = M\omega_0^2 \begin{pmatrix} 3 - 2\cos(k_x) - \cos(\frac{k_x}{2})\cos(\frac{\sqrt{3}k_y}{2}) & \sqrt{3}\sin(\frac{k_x}{2})\sin(\frac{\sqrt{3}k_y}{2}) \\ \sqrt{3}\sin(\frac{k_x}{2})\sin(\frac{\sqrt{3}k_y}{2}) & 3 - 3\cos(\frac{k_x}{2})\cos(\frac{\sqrt{3}k_y}{2}) \end{pmatrix} \quad (\text{S17})$$

The phonon operator is defined as $b_{i,\mathbf{k}} = \sqrt{\frac{M\omega_{i,\mathbf{k}}}{2\hbar}} (U_{i,\mathbf{k}} + \frac{i}{M\omega_{i,\mathbf{k}}} P_{i,\mathbf{k}})$ where $\vec{U}_{\mathbf{k}} = V_{\mathbf{k}}^\dagger \vec{u}_{\mathbf{k}}$ and $\vec{P}_{\mathbf{k}} = V_{\mathbf{k}}^\dagger \vec{p}_{\mathbf{k}}$ are related to the $\vec{p}_{\mathbf{k}}$ and $\vec{u}_{\mathbf{k}}$ through a unitary transformation V that diagonalizes the dynamical matrix as $V^\dagger \mathcal{D}(\mathbf{k}) V = M\omega_0^2 \text{diag}[d_1, d_2]$. The eigenfrequencies of phonon are given by $\omega_{i,\mathbf{k}} = \omega_0 \sqrt{d_i}$. In the particle-hole-symmetric Nambu basis $\psi_p = (b_{1,\mathbf{k}}, b_{2,\mathbf{k}}, b_{1,-\mathbf{k}}^\dagger, b_{2,-\mathbf{k}}^\dagger)^T$, the free phonon Hamiltonian can be written as $H_p = \frac{1}{2} \sum_{\mathbf{k}} \psi_p^\dagger \mathcal{H}_p \psi_p$, where the kernel \mathcal{H}_p is

$$\mathcal{H}_p = \hbar \begin{pmatrix} \omega_{1,\mathbf{k}} & 0 & 0 & 0 \\ 0 & \omega_{2,\mathbf{k}} & 0 & 0 \\ 0 & 0 & \omega_{1,-\mathbf{k}} & 0 \\ 0 & 0 & 0 & \omega_{2,-\mathbf{k}} \end{pmatrix}. \quad (\text{S18})$$

Regarding the free magnon Hamiltonian H_s , we first apply a Schrieffer–Wolff transformation to project the system onto the low-energy subspace. The resulting Hamiltonian retains the same form of Eq. (S14) but with $\eta = 0$. We then perform a Holstein-Primakoff transformation (see below). In reciprocal space, the free magnon Hamiltonian for the SN ground state can be expressed in the Nambu basis $\psi_m = (a_{\mathbf{k}}, a_{-\mathbf{k}}^\dagger)^T$ as $H_s = \frac{1}{2} \sum_{\mathbf{k}} \psi_m^\dagger \mathcal{H}_s \psi_m$, where $a_{\mathbf{k}}^\dagger (a_{\mathbf{k}})$ is the magnon creation (annihilation) operator, and the kernel \mathcal{H}_s takes the form:

$$\mathcal{H}_s = \begin{pmatrix} m_0(\mathbf{k}) & \Sigma(\mathbf{k}) \\ \Sigma^\dagger(\mathbf{k}) & m_0(-\mathbf{k}) \end{pmatrix}. \quad (\text{S19})$$

The off-diagonal term $\Sigma(\mathbf{k})$ involves a summation over the six nearest-neighbor bonds δ of the triangular lattice, given by $\Sigma = m_4 \sum \delta e^{i\mathbf{k}\cdot\delta}$. The diagonal elements are defined by $m_0(\mathbf{k}) = m_1 + m_2(\mathbf{k}) + m_3$. Detailed expressions for $m_{1,2,3,4}$ are provided below. We note that dangling terms (proportional to $a_{\mathbf{k}}$ or $a_{\mathbf{k}}^\dagger$ alone) may appear in H_s ; their presence signals an instability in the assumed SN ground state. The coefficient of such linear terms is $B \sin \phi - 3J^2 \sin 2\phi (1 + \frac{2\Delta D}{J}) / 2D$. Requiring this coefficient to vanish yields two solutions. The first one, $\phi = 0$, is the trivial solution corresponding to the FP phase. The second one, $\phi = \arccos[2BD/3J^2(2 + \frac{4\Delta D}{J})]$, is the non-trivial solution with lower energy for $B_{c,2} < B < B_{c,3}$, which corresponds to the SN phase. The spin configuration defined by this ϕ matches exactly with the one obtained by minimizing the energy in the SN

phase at $\eta = 0$ [Fig. 1(b)]. The existence of this non-trivial solution imposes an upper bound on the magnetic field in the SN phase $B_{max} = 3J^2(2 + \frac{4\Delta D}{J})/2D$, which is found to coincide with the boundary $B_{c,3}$ in the phase diagram [Fig.1(b) of main text]. Consequently, for a large magnetic fields exceeding the limit ($B > B_{max} = B_{c,3}$), only the ferromagnetic FP phase ($\phi = 0$) remains stable, consistent with the phase diagram.

As for the magnon-phonon coupling H_{me} , it does not explicitly depend on the magnetic field. Therefore, the coefficient of magnonic dangling term in H_{me} does not completely vanish as in H_s . Therefore, the lowest order in H_{me} becomes bilinear with respect to magnon and phonon operators:

$$H_{me} = \sum_{\mathbf{k}} \Pi_i(\mathbf{k})(b_{i,\mathbf{k}} + b_{i,-\mathbf{k}}^\dagger)(a_{-\mathbf{k}} + a_{\mathbf{k}}^\dagger) \quad (\text{S20})$$

The repeated subscript i are assumed to be summed. The detailed expression of Π_i can be found below [Eq. (S26)].

In the SN phase, the spins in the effective spin-1/2 space have an ordering wavevector at Γ , which means the smallest unit cell contains one spin site. As shown in the main text, we parametrize the spin axis with a polar angle ϕ as $\hat{\tau}_A = \hat{\tau}_B = \hat{\tau}_C = (\sin \phi, 0, \cos \phi)$. We next adopt the Holstein–Primakoff transformation [46], which is a Hermitian and exact representation for the spin operators:

$$S_i^\dagger = \sqrt{2S} \sqrt{1 - \frac{a_i^\dagger a_i}{2S}}, \quad S_i^\dagger = \sqrt{2S} a_i^\dagger \sqrt{1 - \frac{a_i^\dagger a_i}{2S}}, \quad S_i^z = S - a_i^\dagger a_i \quad (\text{S21})$$

with the constraint $0 \leq a_i^\dagger a_i \leq 2S$ enforced by $-S \leq S^z \leq S$. The tricky part lies in the square root of $a_i^\dagger a_i$. Usually, one adopts the Taylor expansion in the large S limit. However, it's often used also for the case of $S = 1/2$. The justification of this approach comes from the constraint $a_i^\dagger a_i \leq 1$ for $S = 1/2$. More rigorously, the Taylor expansion should be replaced with an exact summation [47], which to the lowest order of magnon operator (ignoring magnon-magnon interaction), is the same as the one obtained from Taylor expansion with higher order terms neglected. Thus, around local spin axis, we are still allowed to use Eq. (S21) for the effective spin-1/2 model. After rotating back to the global coordinates, we have the following Holstein–Primakoff transformation

$$\tau_i^x = \cos \theta_i (a_i + a_i^\dagger)/2 + \sin \theta_i (\frac{1}{2} - a_i^\dagger a_i), \quad \tau_i^y = (a_i - a_i^\dagger)/(2i), \quad \tau_i^z = \cos \theta_i (\frac{1}{2} - a_i^\dagger a_i) - \sin \theta_i (a_i + a_i^\dagger)/2 \quad (\text{S22})$$

with $\theta_i = \phi$ for all the spin sites in the SN phase as we have mentioned. Then, after a tedious calculation, the free magnon Hamiltonian in the reciprocal space is found to be

$$H_s = \frac{1}{2} \sum_{\mathbf{k}} \Psi_m^\dagger \begin{pmatrix} m_0(\mathbf{k}) & 2m_4 \sum_{\delta} e^{i\mathbf{k} \cdot \delta} \\ 2m_4 \sum_{\delta} e^{-i\mathbf{k} \cdot \delta} & m_0(-\mathbf{k}) \end{pmatrix} \Psi_m, \quad (\text{S23})$$

where the Nambu basis is $\Psi_m = (a_{\mathbf{k}}, a_{-\mathbf{k}}^\dagger)$. The m_i , $i \in (1, 2, 3, 5)$ terms involved in the Hamiltonian are given by

$$\begin{aligned} m_0(k) &= m_1 + m_2 + m_3 \\ m_1 &= -\frac{12J^2}{D} \left(\frac{\cos 2\phi}{4} + \frac{\Delta D}{J} \cos^2 \phi \right) \\ m_2 &= -\frac{J^2}{D} \left[\frac{\cos 2\phi + 1}{4} - \frac{\Delta D}{J} \sin^2 \phi \right] \sum_{\delta} \cos(\mathbf{k} \cdot \delta) \\ m_3 &= 2g_c \mu_B B \cos \phi \\ m_4 &= -\frac{J^2}{2D} \left[\frac{\cos 2\phi - 1}{4} - \frac{\Delta D}{J} \sin^2 \phi \right] \end{aligned}$$

where the summation for dimensionless δ runs over the six nearest-neighbor bond direction of triangular lattice. The linear terms (dangling terms) of free magnon Hamiltonian must vanish for a stable ground state, which enforces the following condition

$$g_c \mu_B B \sin \phi - \frac{3J^2 \sin 2\phi}{4D} \left(2 + \frac{4\Delta D}{J} \right) = 0, \quad (\text{S24})$$

whose nontrivial solution determines the ground state of τ in the SN phase.

The total Hamiltonian $H = H_s + H_p + H_{me}$ can then be written in the enlarged Nambu basis $\psi =$

$(b_{1,\mathbf{k}}, b_{2,\mathbf{k}}, b_{1,-\mathbf{k}}^\dagger, b_{2,-\mathbf{k}}^\dagger, a_{\mathbf{k}}, a_{-\mathbf{k}}^\dagger)^T$ as $H = \frac{1}{2} \sum_{\mathbf{k}} \psi^\dagger \mathcal{H}^{SN} \psi$, where the kernel can be written in the block matrix form

$$\mathcal{H}^{SN} = \begin{pmatrix} \mathcal{H}_p(\mathbf{k}) & \Pi^\dagger(\mathbf{k}) \\ \Pi(\mathbf{k}) & \mathcal{H}_s(\mathbf{k}) \end{pmatrix} \quad (\text{S25})$$

Here, the phonon kernel has a diagonal form $\mathcal{H}_p = \text{diag}[\omega_{1,\mathbf{k}}, \omega_{2,\mathbf{k}}, \omega_{1,-\mathbf{k}}, \omega_{2,-\mathbf{k}}]$. The off-diagonal block $\Pi(\mathbf{k}) = \begin{pmatrix} \Pi_1 & \Pi_2 & \Pi_1 & \Pi_2 \\ \Pi_1 & \Pi_2 & \Pi_1 & \Pi_2 \end{pmatrix}$ comes from the H_{me} , and the matrix element $\Pi_i(\mathbf{k})$ is

$$\Pi_j(\mathbf{k}) = -i[d_{j,\mathbf{k}}]^{-1/4} \sqrt{\frac{\hbar \omega_0 \eta}{2J}} \frac{J^2 \sin 2\phi}{8D} \left(2 + \frac{4\Delta D}{J}\right) \sum_{\delta} \sin(\mathbf{k} \cdot \delta) \delta_i V_{ij} \quad (\text{S26})$$

SPIN-NEMATIC-SUPERSOLID PHASE

In SNS phase, we enlarge the unit cell for phonon to be the same as the magnon. This makes the dynamical matrix \mathcal{D} to be a 6×6 matrix with involved expression. The dynamical matrix \mathcal{D} can be read off from the expression for free phonon Hamiltonian in the reciprocal space

$$H_p = \sum_{\mathbf{k}, \alpha \in A, B, C} \frac{p_{\alpha,\mathbf{k}}^2}{2M} + \frac{M\omega_0^2}{2} \sum_{\mathbf{k}, \alpha \in A, B, C} \sum_{\delta^{\alpha\beta}}^{\beta \neq \alpha} (\delta^{\alpha\beta} \cdot \mathbf{u}_{\alpha,\mathbf{k}}^\dagger) (\delta^{\alpha\beta} \cdot \mathbf{u}_{\alpha,\mathbf{k}}) + (\delta^{\alpha\beta} \cdot \mathbf{u}_{\beta,\mathbf{k}}^\dagger) (\delta^{\alpha\beta} \cdot \mathbf{u}_{\beta,\mathbf{k}}) \quad (\text{S27})$$

The particle-hole-symmetric Nambu basis for the phonon in the enlarge unit cell is $\psi_p = \psi_p^- \oplus \psi_p^+$ with $\psi_p^- = (b_{1,\mathbf{k}}, \dots, b_{6,\mathbf{k}})^T$ and $\psi_p^+ = (b_{1,-\mathbf{k}}^\dagger, \dots, b_{6,-\mathbf{k}}^\dagger)^T$. The free phonon Hamiltonian then reads $H_p = \frac{1}{2} \sum_{\mathbf{k}} \psi_p^\dagger \mathcal{H}_p \psi_p$, where the kernel \mathcal{H}_p is

$$\mathcal{H}_p = \hbar \text{diag}[\omega_{1,\mathbf{k}}, \dots, \omega_{6,\mathbf{k}}, \omega_{1,-\mathbf{k}}, \dots, \omega_{6,-\mathbf{k}}]. \quad (\text{S28})$$

Here, the eigenfrequency ω_i can be obtained by unitary diagonalizing the 6×6 dynamical matrix \mathcal{D} . In Fig. S1(b), we plot the free phonon band spectra along the Γ -M-K- Γ path of the reduced BZ [green dashed line in Fig. S1(a)]. While in Fig. S1(c), free phonon band spectra is plotted along the same Γ -M-K- Γ path but of the original BZ [blue dashed line in Fig. S1(a)]. Note that in both cases, we have six bands in total. By projecting out the fictitious optical modes (see next section) in the original BZ, we obtain Fig. S1(d), which is in full agreement of the free phonon spectra (blue lines of Fig.2 in the main text). The band spectra of the main text are plotted along the original BZ for phonon [Blue dashed lines].

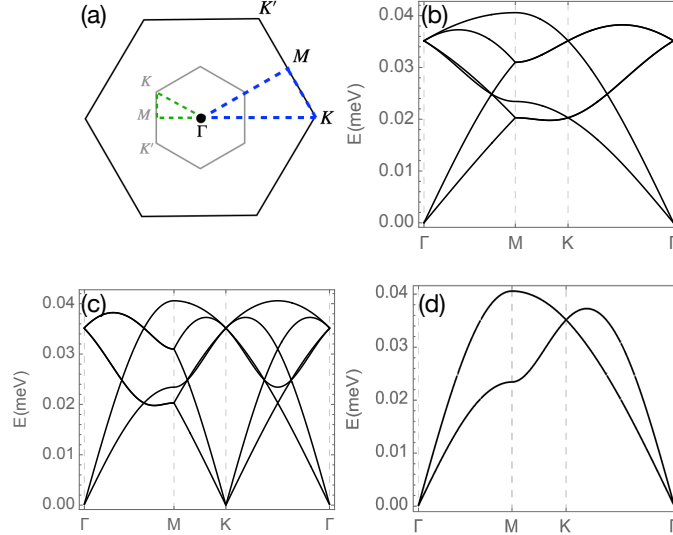


FIG. S1. (a) The original BZ (black solid lines) of the triangular lattice and the reduced BZ (gray solid line) corresponding to the enlarged unit cell in the SNS phase. (b) Free phonon band structure along the green dashed path. (c) Free phonon band structure along the blue dashed path. (d) Same as (c), but with the fictitious optical modes removed by projection P^{ac} .

As for the free magnon Hamiltonian H_s , we use the basis $\psi_m = \psi_m^- \oplus \psi_m^+$ with $\psi_m^- = (a_{A,\mathbf{k}}, a_{B,\mathbf{k}}, a_{C,\mathbf{k}})^T$ and $\psi_m^+ = (a_{A,-\mathbf{k}}, a_{B,-\mathbf{k}}, a_{C,-\mathbf{k}})^T$. Here, a_α^\dagger is the magnon creation operator in the $\alpha \in (A, B, C)$ sublattice. We have three bands (three sublattice) for magnon in total. We follow the same procedure as in the SN phase and the free magnon Hamiltonian H_s can be written as $H_s = \frac{1}{2} \sum_{\mathbf{k}} \psi_m^\dagger \mathcal{H}_s \psi_m$, where the expression of the kernel \mathcal{H}_s becomes very involved and the full expression is provided in Eq. (S29). By writing the Hamiltonian H_s in such quadratic form we have assumed that the dangling terms vanish for a stable SNS ground state. The vanishing condition contains two transcendental equations for the angle θ_1 and θ_2 [see Eq. (S30) below]. The first solution gives $\theta_1 = 0, \theta_2 = \pi$, which is the trivial one and corresponds to the UUD phase. The second solution is the nontrivial one and has the lower energy for $B < B_{c,1}$, which corresponds to the SNS phase. Again, we found that such nontrivial solution exactly matches the one obtained from minimizing the energy in the SNS phase of Fig.1(b) in the main text. Additionally, the existence of the nontrivial solution (SNS phase) imposes an upper bound B_{max} of the magnetic field for the SNS phase, which is found to exactly match the threshold $B_{max} = B_{c,1}$ in the phase diagram of the main text.

The SNS phase is characterized by $\hat{\tau}_A = \hat{\tau}_B = (\sin \theta_1, 0, \cos \theta_1)$, $\hat{\tau}_C = (\sin \theta_2, 0, \cos \theta_2)$ with ordering wavevector at K . Utilizing Eq. (S22) and after a tedious calculation, the kernel \mathcal{H}_s of free magnon Hamiltonian is found be

$$\mathcal{H}_s = \begin{pmatrix} d_1 & m_1^+ f_{AB} & m_{12}^+ f_{AC} & 0 & m_1^- f_{AB} & m_{12}^- f_{AC} \\ m_1^+ f_{AB}^* & d_1 & m_{12}^+ f_{BC} & m_1^- f_{AB}^* & 0 & m_{12}^- f_{BC} \\ m_{12}^+ f_{AC}^* & m_{12}^+ f_{BC}^* & d_2 & m_{12}^- f_{AC}^* & m_{12}^- f_{BC}^* & 0 \\ 0 & m_1^- f_{AB} & m_{12}^- f_{AC} & d_1 & m_1^+ f_{AB} & m_{12}^+ f_{AC} \\ m_1^- f_{AB}^* & 0 & m_{12}^- f_{BC} & m_1^+ f_{AB}^* & d_1 & m_{12}^+ f_{BC} \\ m_{12}^- f_{AC}^* & m_{12}^- f_{BC}^* & 0 & m_{12}^+ f_{AC}^* & m_{12}^+ f_{BC}^* & d_2 \end{pmatrix} \quad (\text{S29})$$

where the $f_{\alpha\beta}$, $\alpha, \beta \in (A, B, C)$ terms are given by $f_{\alpha\beta} = -\frac{J^2}{D} \sum_{\delta\alpha\beta} e^{i\mathbf{k}\cdot\delta\alpha\beta}$. The summation $\sum_{\delta\alpha\beta}$ involves three bond directions that connect the nearest-neighboring sites α and β ($\alpha \neq \beta$). The coefficient in the kernel \mathcal{H}_s are

$$\begin{aligned} m_1^\pm &= \frac{\cos(2\theta_1) \pm 1}{4} - \frac{\sin^2 \theta_1 \Delta D}{J} \\ m_{12}^\pm &= \left[\frac{\cos(\theta_1 + \theta_2) \pm 1}{4} - \frac{\Delta D}{J} \sin \theta_1 \sin \theta_2 \right] \\ d_1 &= -\frac{J^2}{D} [n_1 + n_{12}] + 2g_c \mu_B B \cos \theta_1 \\ d_2 &= -2\frac{J^2}{D} n_{12} + 2g_c \mu_B B \cos \theta_2 \\ n_1 &= 3 \left[\frac{\cos 2\theta_1}{2} + 2 \cos^2 \theta_1 \frac{\Delta D}{J} \right] \\ n_{12} &= 3 \left[\frac{\cos(\theta_1 + \theta_2)}{2} + \frac{2\Delta D}{J} \cos \theta_1 \cos \theta_2 \right] \end{aligned}$$

Again, the linear terms (dangling terms) of free magnon Hamiltonian must vanish for a stable ground state, which enforces the following condition

$$-\frac{3J^2}{D} \left[\frac{\sin(\theta_1 + \theta_2) + \sin 2\theta_1}{4} + \frac{\sin \theta_1 \Delta D}{J} (\cos \theta_2 + \cos \theta_1) \right] + g_c \mu_B B \sin \theta_1 = 0 \quad (\text{S30a})$$

$$-\frac{3J^2}{D} \left[\frac{\sin(\theta_1 + \theta_2)}{2} + \frac{2 \cos \theta_1 \sin \theta_2 \Delta D}{J} \right] + g_c \mu_B B \sin \theta_2 = 0 \quad (\text{S30b})$$

The nontrivial solution of above two transcendental equation determines the ground state of τ in the SNS phase.

The magnon-phonon coupling terms have three contribution from the three sublattice $H_{me} = \sum_{\alpha \in (A, B, C)} H_{me}^\alpha$ with H_{me}^α given by

$$H_{me}^\alpha = \sum_{\mathbf{k}} [d_j]^{-\frac{1}{4}} [G_\alpha]_i [V]_{ij} (b_{j,\mathbf{k}} + b_{j,-\mathbf{k}}^\dagger) (a_{\alpha,-\mathbf{k}} + a_{\alpha,\mathbf{k}}^\dagger), \quad (\text{S31})$$

where the matrix V diagonalizes the dynamical matrix \mathcal{D} of the phonon as $V^\dagger \mathcal{D}(\mathbf{k}) V = M \omega_0^2 \text{diag}[d_1, \dots, d_6]$. The vectors G_α

are

$$\begin{aligned}\mathbf{G}_A &= -\frac{J^2}{D} \sqrt{\frac{\hbar\omega_0\eta}{2J}} (0, 0, sp_1 g_{AB}^x, sp_1 g_{AB}^y, sp_2 g_{AC}^x, sp_2 g_{AC}^y) \\ \mathbf{G}_B &= \frac{J^2}{D} \sqrt{\frac{\hbar\omega_0\eta}{2J}} (sp_1 [g_{AB}^*]^x, sp_1 [g_{AB}^*]^y, 0, 0, sp_2 g_{BC}^x, sp_2 g_{BC}^y) \\ \mathbf{G}_C &= \frac{J^2}{D} \sqrt{\frac{\hbar\omega_0\eta}{2J}} (sp_3 [g_{AC}^*]^x, sp_3 [g_{AC}^*]^y, sp_3 [g_{BC}^*]^x, sp_3 [g_{BC}^*]^y, 0, 0),\end{aligned}$$

where the vectors of structure factor are $\mathbf{g}_{\alpha\beta} = \sum_{\delta\alpha\beta} e^{i\mathbf{k}\cdot\delta\alpha\beta} \delta^{\alpha\beta}$. The summation involves three bond directions that connect the nearest-neighboring sites α and β ($\alpha \neq \beta$). The coefficients are appearing in \mathbf{G}_α are

$$\begin{aligned}sp_1 &= \left(2 + \frac{4\Delta D}{J}\right) \frac{\sin 2\theta_1}{8} \\ sp_2 &= \left[\frac{\cos \theta_1 \sin \theta_2}{4} + \frac{\sin \theta_1 \cos \theta_2}{4} \left(1 + \frac{4\Delta D}{J}\right)\right] \\ sp_3 &= \left[\frac{\sin \theta_1 \cos \theta_2}{4} + \frac{\cos \theta_1 \sin \theta_2}{4} \left(1 + \frac{4\Delta D}{J}\right)\right]\end{aligned}$$

The total Hamiltonian $H = H_s + H_p + H_{me}$ can then be written in the enlarged Nambu basis $\psi = \psi_p \oplus \psi_m$ as $H = \frac{1}{2} \sum_{\mathbf{k}} \psi^\dagger \mathcal{H}^{SNS} \psi$, where the kernel can be written in the block matrix form

$$\mathcal{H}^{SNS} = \begin{pmatrix} \mathcal{H}_p(\mathbf{k}) & \Pi^\dagger(\mathbf{k}) \\ \Pi(\mathbf{k}) & \mathcal{H}_s(\mathbf{k}) \end{pmatrix} \quad (\text{S32})$$

Here, the off diagonal block $\Pi(\mathbf{k})$ is a 6×12 matrix, whose elements can be easily read off from the Eq. (S31). To retrieve the particle-hole symmetry, we first transform our enlarged Nambu basis $\psi = \psi_p \oplus \psi_m$ to a particle-hole symmetric basis $\Psi = \Lambda \psi$, which results in a particle-hole symmetric Hamiltonian $\mathcal{H}_{p-h}^{SNS} = (\Lambda^{-1})^\dagger \mathcal{H}^{SNS} \Lambda^{-1}$. The generalized eigenvalue problem becomes $\mathcal{H}_{p-h}^{SNS} Q = gQ\bar{\epsilon}$ with the metric $g = \sigma_z \otimes I_{9 \times 9}$ and $\bar{\epsilon} = g\epsilon$.

PROJECTION OPERATORS

The projection operator for the acoustic phonon comes naturally from the vibration characteristic at long-wave-length limit ($\mathbf{k} \rightarrow \mathbf{0}$), where the uniform displacement of all sites corresponds to the lattice translational symmetry. Consequently, in the basis of $\psi_u = (u_A^x, u_A^y, u_B^x, u_B^y, u_C^x, u_C^y)$, the normalized projection operator P^u for the acoustic mode has the form $P_u = P_u^x (P_u^x)^\dagger + P_u^y (P_u^y)^\dagger$ with $P_u^x = (1, 0, 1, 0, 1, 0)^T / \sqrt{3}$ and $P_u^y = (0, 1, 0, 1, 0, 1)^T / \sqrt{3}$. P_u^x and P_u^y correspond to the uniform vibration along x and y directions, respectively. Taking the expression for P_u^x and P_u^y into P_u , we obtain

$$P_u = \frac{1}{3} \begin{pmatrix} 1 & 0 & 1 & 0 & 1 & 0 \\ 0 & 1 & 0 & 1 & 0 & 1 \\ 1 & 0 & 1 & 0 & 1 & 0 \\ 0 & 1 & 0 & 1 & 0 & 1 \\ 1 & 0 & 1 & 0 & 1 & 0 \\ 0 & 1 & 0 & 1 & 0 & 1 \end{pmatrix} \quad (\text{S33})$$

In the particle-hole symmetric Nambu basis $\psi_p = (b_{1,\mathbf{k}}, \dots, b_{6,\mathbf{k}}, b_{1,-\mathbf{k}}^\dagger, \dots, b_{6,-\mathbf{k}}^\dagger)^T$, the projection operator for acoustic mode then becomes $P_p = (V^\dagger p_r V) \oplus (V^\dagger p_r V)$, where the unitary V comes from changing the basis from ψ_u to ψ_p and the direction sum comes from the hole sector. Note that the Hamiltonian (S32) is written in the enlarged Nambu basis $\psi = \psi_p \oplus \psi_m$ with magnon Nambu basis $\psi_m = (a_{A,\mathbf{k}}, a_{B,\mathbf{k}}, a_{C,\mathbf{k}}, a_{A,-\mathbf{k}}^\dagger, a_{B,-\mathbf{k}}^\dagger, a_{C,-\mathbf{k}}^\dagger)$. To retrieve the particle-hole symmetry for the basis and obtain

a generalized eigenvalue problem, we need transform our enlarged Nambu basis $\psi = \psi_p \oplus \psi_m$ to a particle-hole symmetric basis

$$\Psi \equiv \begin{pmatrix} b_{1,k} \\ \vdots \\ b_{6,k} \\ a_{A,k} \\ a_{B,k} \\ a_{C,k} \\ b_{1,-k}^\dagger \\ \vdots \\ b_{6,-k}^\dagger \\ a_{A,-k}^\dagger \\ a_{B,-k}^\dagger \\ a_{C,-k}^\dagger \end{pmatrix} = \Lambda(\psi_p \oplus \psi_m) = \begin{pmatrix} I_6 & 0 & 0 & 0 & 0 \\ 0 & 0 & 0 & I_3 & 0 \\ 0 & I_3 & 0 & 0 & 0 \\ 0 & 0 & I_3 & 0 & 0 \\ 0 & 0 & 0 & 0 & I_3 \end{pmatrix} \begin{pmatrix} b_{1,k} \\ \vdots \\ b_{6,k} \\ b_{1,-k}^\dagger \\ \vdots \\ b_{6,-k}^\dagger \\ a_{A,k} \\ a_{B,k} \\ a_{C,k} \\ a_{A,-k}^\dagger \\ a_{B,-k}^\dagger \\ a_{C,-k}^\dagger \end{pmatrix} \quad (\text{S34})$$

Then, in the particle-hole symmetric Nambu Ψ , the projection operator for the acoustic phonon P^{ax} takes the final form

$$P^{ac} = (\Lambda^{-1})^\dagger [(V^\dagger p_r V) \oplus (V^\dagger p_r V) \oplus 0_{6 \times 6}] \Lambda^{-1} \quad (\text{S35})$$

Note that, the above operator also projects out the magnon bands. To keep the magnon band and simultaneously remove the fictitious optical phonon bands, we can replace the last $0_{6 \times 6}$ matrix with identity matrix $I_{6 \times 6}$. The projection operator we constructed works very well where in Fig. S1(d) we can see that four bands are completely removed and the remaining two bands are exactly the acoustic phonon bands. In Figs.4(c,f) of the main text, each band is plotted with the transparency weight given by $T_n = Q_n^\dagger g P^{ax} Q_n$ such that the fictitious optical modes will become invisible (removed). Here, Q_n is the n -th column of eigenstate matrix Q for the particle-hole symmetric Hamiltonian $\mathcal{H}_{p-h}^{SNS} = (\Lambda^{-1})^\dagger \mathcal{H}^{SNS} \Lambda^{-1}$.

To visualize the phonon-magnon hybridization, we plot the band spectra with color gradients representing the normalized relative weights of the phonon-like (blue) and magnon-like (red) components for the n -th band. The weights are defined as $w_a^n = Q_n^\dagger g P_a Q_n$ and $w_b^n = Q_n^\dagger g P_b Q_n$, where Q_n is the n -th column of the transformation (eigenstate) matrix Q , and $P_{a/b}$ are the normalized projection operators for the magnon and phonon subspaces, respectively. In the particle-hole symmetric Nambu Ψ , the projection operator for phonon-like P_b and magnon-like P_a components is straightforwardly given by $P_b = \text{diag}[1, \dots, 1, 0, 0, 0, 1, \dots, 1, 0, 0, 0]$ and $P_a = \text{diag}[0, \dots, 0, 1, 1, 1, 0, \dots, 0, 1, 1, 1]$. These weights satisfy the normalization condition $w_a^n + w_b^n = Q_n^\dagger g Q_n = 1$ (since $P_a + P_b = I$) for the bands in the particle sectors with positive energy. As illustrated in Fig.2 of main text, the bands near the avoided crossing appear green, signifying strong hybridization between magnon and phonon states. We note that while a finite η does not open a gap at the Γ point, the eigenstates in its vicinity exhibit mixed character (green color) at high magnetic fields [Fig.2(f) of main text], indicating presence of hybridization despite the absence of an avoided crossing gap.